remote sensing

MDPI

Technical Note

Improving Mean Minimum and Maximum Month-to-Month Air Temperature Surfaces Using Satellite-Derived Land Surface Temperature

Maria Mira [1,*], Miquel Ninyerola [2], Meritxell Batalla [3], Lluís Pesquer [3] and Xavier Pons [1]

1 GRUMETS Research Group, Department of Geography, Edifici B, Universitat Autònoma de Barcelona, 08193 Bellaterra, Catalonia, Spain; xavier.pons@uab.cat
2 GRUMETS Research Group, Department of Animal Biology, Plant Biology and Ecology, Universitat Autònoma de Barcelona, 08193 Bellaterra, Catalonia, Spain; miquel.ninyerola@uab.cat
3 GRUMETS Research Group, CREAF, Edifici C, Universitat Autònoma de Barcelona, 08193 Bellaterra, Catalonia, Spain; meritxell.batalla@creaf.uab.cat (M.B.); l.pesquer@creaf.uab.cat (L.P.)
* Correspondence: maria.mira@uab.cat; Tel.: +34-93-581-3273

Received: 19 October 2017; Accepted: 11 December 2017; Published: 14 December 2017

Abstract: Month-to-month air temperature (T_{air}) surfaces are increasingly demanded to feed quantitative models related to a wide range of fields, such as hydrology, ecology or climate change studies. Geostatistical interpolation techniques provide such continuous and objective surfaces of climate variables, while the use of remote sensing data may improve the estimates, especially when temporal resolution is detailed enough. The main goal of this study is to propose an empirical methodology for improving the month-to-month T_{air} mapping (minimum and maximum) using satellite land surface temperatures (LST) besides of meteorological data and geographic information. The methodology consists on multiple regression analysis combined with the spatial interpolation of residual errors using the inverse distance weighting. A leave-one-out cross-validation procedure has been included in order to compare predicted with observed values. Different operational daytime and nighttime LST products corresponding to the four months more characteristic of the seasonal dynamics of a Mediterranean climate have been considered for a thirteen-year period. The results can be considered operational given the feasibility of the models employed (linear dependence on predictors that are nowadays easily available), the robustness of the leave-one-out cross-validation procedure and the improvement in accuracy achieved when compared to classical T_{air} modeling results. Unlike what is considered by most studies, it is shown that nighttime LST provides a good proxy not only for minimum T_{air}, but also for maximum T_{air}. The improvement achieved by the inclusion of remote sensing LST products was higher for minimum T_{air} (up to 0.35 K on December), especially over forests and rugged lands. Results are really encouraging, as there are generally few meteorological stations in zones with these characteristics, clearly showing the usefulness of remote sensing to improve information about areas that are difficult to access or simply with a poor availability of conventional meteorological data.

Keywords: air surface temperature; land surface temperature; spatial interpolation; climatological modeling; remote sensing

1. Introduction

The surface air temperature (hereafter T_{air}) is defined as the temperature measured by a thermometer exposed to the air in a place protected from direct solar radiation, normally located at about 1.5 m above surface level on land [1]. The T_{air} is a key climatic and meteorological variable that makes it possible to quantify biophysical processes at surface level, such as energy flows, actual and

potential evapotranspiration, water stress, and species distribution [2–6]. Further, it is used in many environmental applications, including vector-borne disease bionomics [7], terrestrial hydrology [8], biosphere processes [9] and climate change [10]. In addition to mean T_{air}, minimum and maximum values are central to understanding these biosphere processes, and are often preferred measurements.

T_{air} is measured at meteorological stations, which provide accurate (although data filtering and quality control are very important) temporally discrete information that is spatially characterized by the density and distribution of the network of available stations. Hence, these stations have limited ability to describe the spatial heterogeneity of T_{air} over large areas of the Earth, especially in regions with complex topographies and landscapes. Therefore, there are many studies on climate interpolation methods using meteorological data that may or may not include geographical variables as predictors.

Using information obtained from airborne sensors or artificial satellites (remote sensing) to observe the Earth from space is the only methodology that effectively evaluates the spatial distribution of land surface variables on a regional and global scale. Thanks to the technological developments in the latest generation of spectral band sensors in the thermal infrared region (8–14 μm) (e.g., Sentinel-3, Landsat, Moderate Resolution Imaging Spectroradiometer (MODIS), Advanced Spaceborne Thermal Emission and Reflection Radiometer (ASTER), Advanced Along Track Scanning Radiometer (AATSR), and Advanced Very High Resolution Radiometer (AVHRR)), the capacity of existing Earth observation programs has improved. These sensors incorporate new spectral measurement channels and provide much better spatial and spectral resolution than just a few decades ago. Likewise, the long historical satellite data series that exist today (Landsat, over 40 years; NOAA-AVHRR, over 30 years; MODIS, 16 years) make it possible to combine climate cartography based on data from meteorological stations with satellite information [11–15].

Land surface temperature (LST) retrieved from thermal infrared remote sensing measurements has been frequently used to estimate T_{air} [13,14,16–23]. The LST is closely related to the surface energy balance and the water status of the Earth's surface. It mainly depends on the amount of radiative energy that the surface absorbs, the partitioning of heat in sensible and latent heat fluxes, and the characteristics of the atmosphere close to the ground (in particular T_{air} and turbulence) [24].

The level of precision generally accepted as "accurate" for T_{air} estimates based on remote sensing is between 1 and 2 °C [25]. A review can be found in [26] of the methods commonly used to estimate T_{air} based on LST. These authors divided the methods into three distinct groups: (1) statistical approaches based on regression techniques [21,27–29]; (2) temperature-vegetation index [4,30]; and (3) energy-balance approaches [12,31]. The methodology applied in our study is based on geostatistical interpolation techniques and we combine long meteorological series of T_{air} with geographical variables, and LST remote sensing estimates. This methodology has been extensively tested in previous studies [32–34] that model Iberian Peninsula T_{air} and precipitation for monthly and annual periods using only geographical variables. There are also many works that use LST to predict T_{air}, considering daily or instantaneous T_{air} for short time scales (generally one year) [4,12,20,21,23,26,27,35–39]. Nevertheless, here we will focus on estimating monthly T_{air} (similarly to [40]) for a long time series (similarly to recently published works by [41–43]).

The present work has the general aim of progressing in the understanding and prediction of future environmental changes. The main objective is to improve the monthly T_{air} spatial estimates (minimum and maximum) currently provided by Geographic Information Systems (GIS)-based models that combine statistical (multiple regression) and spatial interpolation of the regression residuals. T_{air} data have been obtained from meteorological stations but we have added LST from satellite data as a predictor. In this study, we use a long and robust time series (from 2003 to 2015) that includes data from both conventional meteorological observations and remote sensing as well as geographic factors such as altitude, latitude and continentality, etc., and that also takes into account LST products from different satellites. Our objective is to demonstrate that long-term LST averages could be useful to improve long-term averaged climate maps. Some previous works [4,12,20,21,23,26,27,35–39] incorporate instantaneous, hourly or daily LST values to build detailed time-resolution climate surfaces,

and LST information is very useful in these scenarios because the geographic predictors are less important in a daily or sub-daily basis where specific atmospheric states could be more significant to quantify temperature.

We have focussed particularly on detecting when and in which cases LST could improve the GIS-based maps, especially for minimum and maximum T_{air} for which it is not enough to use just DEM-related variables to obtain reliable digital temperature surfaces. Changes in the T_{air} estimates at the spatial and temporal levels were evaluated considering the analysis of data from the different times of the year as well as the differentiation between land cover and levels of orographic complexity of the territory.

2. Study Area

The study area corresponds to Catalonia, northeastern Iberian Peninsula on the Mediterranean coast, centered at 1°40′ of east longitude and 41°44′ of north latitude and with an approximate area of 32,106 km^2 (see Figure 1). This region is characterized by a heterogeneous orography with elevations ranging from sea level to about 3000 m. It has variable water availability both intra-annually and inter-annually due to repeated drought periods. The climate is typically Mediterranean. The Pyrenees and the neighboring areas have a high-altitude climate, with abundant snow and minimum temperatures below 0 °C in winter, and an annual rainfall above 1000 mm. Along the coast, the climate is mild and temperate with temperatures increasing from north to south, while the rain follows the opposite gradient. The inland areas have a continental Mediterranean climate, with colder winters and hotter summers than coastal areas [44].

Catalonia is composed by four main vegetation units. The first is Mediterranean vegetation, which covers most of the surface area of Catalonia and is dominated by sclerophyllous evergreen forests ranging from sea level to 1000 m. The second is Eurosiberian vegetation dominated by deciduous broad-leaved forests ranging from 1000 to 1600 m. The third is subalpine vegetation dominated by needle-leaf evergreen conifers from 1600 to 2200 m, and the fourth is the Boreoalpine vegetation dominated by grasslands in areas higher than 2200 m [45]. Almost 38% of Catalonia's surface is covered by forests (including evergreen forests, deciduous broad-leaved forests and mixed forests). Another important category is crops, which represent 34.4% of the surface. The third most abundant cover is shrublands (16.4%) followed by grassland (4%), urban (3%), inland water (1.6%), and other minor categories such as roads, bare soils, etc. (2.6%) [46].

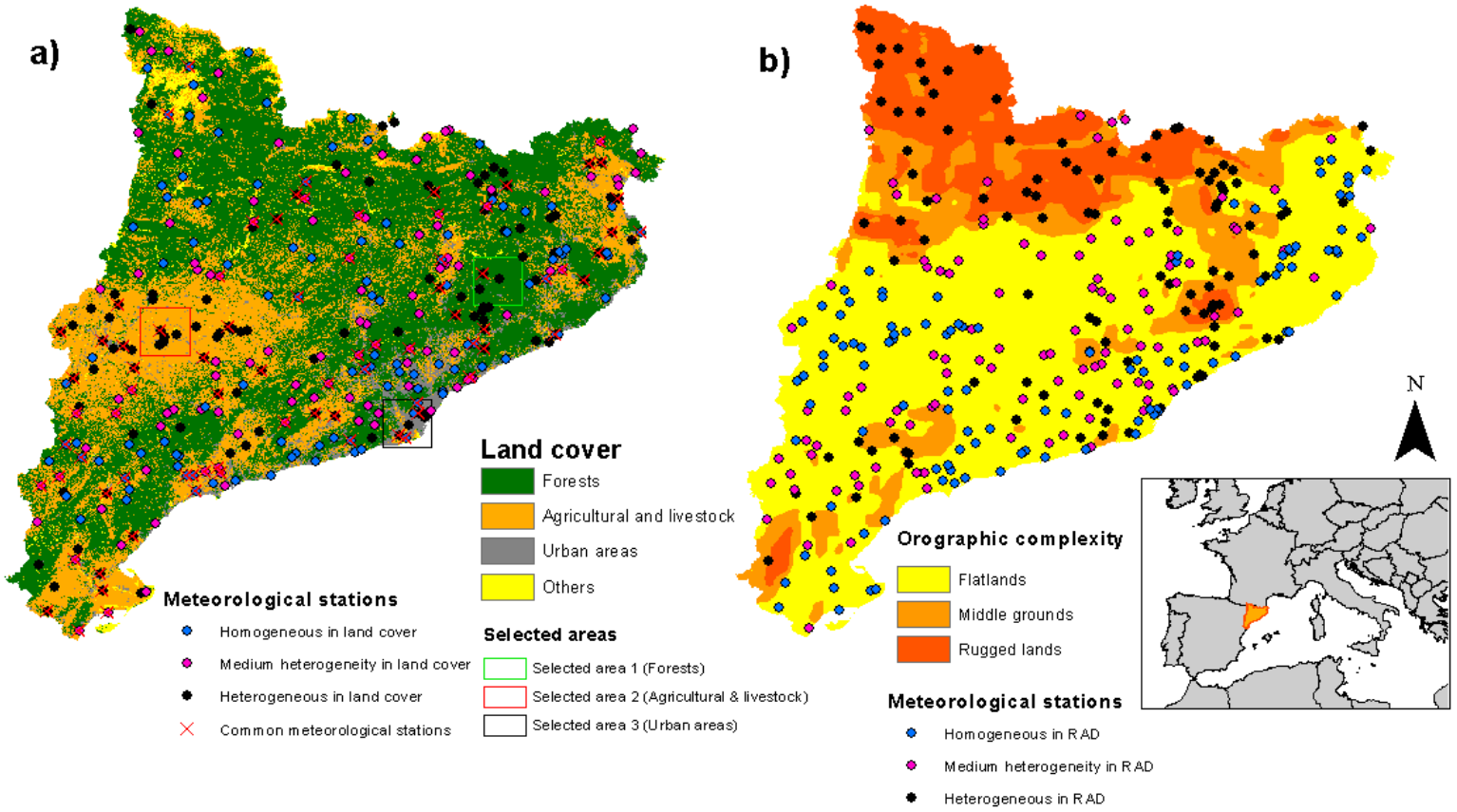

Figure 1. General view of Catalonia, northeast Iberian Peninsula, in Universal Transversal Mercator (UTM) projection. Classification in terms of: (**a**) land cover; and (**b**) orographic complexity are shown. The land cover map has been developed using orthophotographs obtained in 2009. The geographic location of the filtered meteorological stations is also shown, classified in terms of the heterogeneity level in: land cover (**a**) and; potential solar radiation (**b**), as well as the identification of meteorological stations common to all months (**a**). Three selected areas of the image, characteristic of a predominant land cover, are also identified. Because each month and case has a different number of meteorological stations, we represented the case with the maximum number of meteorological stations (maximum T_{air} in March 2014).

3. Materials

The common temporal range used in the study, in accordance with the availability of satellite data, is from 2003 to 2011, while it extended to 2015 in the case of MODIS data. We selected four months to analyze the seasonal dynamics that correspond to a Mediterranean climate (detailed in the previous section), corresponding to the months of the equinoxes and solstices: March, June, September and December. The different datasets used are explained below and summarized in Table 1.

Table 1. Data used in the approach, together with its source or the name of the product, the date and the resolution/density.

Data		Source or Product Name	Dates	Density/Resolution
Meteorological station data		AEMET (www.aemet.es) SMC (www.meteo.cat)	2003–2015	179–329 stations for each month
Other geographic data	Digital Elevation Model	Cartographic Institute of Catalonia (www.icgc.cat)	2004–2007	15 m
Satellite LST	MODIS	MOD11B3 and MYD11B3	2003–2015	5568 m
	AATSR and ATSR-2	ATSR LST Climate Data Record Level-3	2003–2011	0.05°

3.1. Meteorological Station Data

Month-to-month temperature records were obtained from the meteorological stations of the Spanish National Meteorological Agency (AEMET) [47] and the Catalan Meteorological Service (SMC) [48]. For long-term climatology, it is important to submit the data series to a rigorous quality control before mapping; this control has to be highly accurate to avoid unnecessary losses of spatial coverage while removing outliers that could negatively affect the resulting maps. In our case, spatio-temporal outlier detection was based on removing records outside three standard deviations from the mean values, combining the temporal perspective (one record was compared with all the records for the same station and for a specific month) with the spatial perspective (one record was compared with surrounding stations for a specific month and year). Finally, records that did not fulfill these two criteria were removed from the database.

In addition to removing outliers, we used expert knowledge (quality of the station series, position accuracy, etc.) and statistical indicators (robustness of the series based on the standard deviation of the number of monthly records) for the complete period of the series and for the studied period (2003–2015). Finally, to avoid artifacts in the interpolation step due to the proximity of some stations, a criterion of minimum distance (1 km) was applied. The criteria used to choose one of the stations closer than 1 km was based on the series that was longest and most robust. Once stations and/or records had been filtered, we selected the meteorological stations with temperature series longer than 15 years (considering the complete meteorological series for each station) or at least longer than 10 years in the studied period. This criterion was relaxed for recent stations with less than 10 years of records.

After applying the filter criterion, an average of 224 stations for each month were considered, varying between a minimum of 179 and a maximum of 329. Figure 1 shows the spatial distribution of these meteorological stations over the study area for the month with the maximum number of stations, as well as the 80 meteorological stations common for all cases. The minimum and maximum T_{air} values were observed around 5:00–6:00 a.m. and 3:00–4:00 p.m. local time respectively, although there was some variability depending on the location and time of the year. The accuracy of the T_{air} measurements was 0.1 K.

3.2. Other Geographic Data

The geographic variables were chosen taking into account their influence on the climate. We used variables whose influence is well documented in the bibliography (altitude and latitude). In addition,

continentality, potential solar radiation and a topographic wetness index were also included to model the complexity of the climate in mountain areas. All variables were obtained from a Digital Elevation Model (DEM) and from different GIS analysis procedures.

Altitude (Alt.) is the nominal altitude above sea level of the stations, and it gives information on the variability caused by the relief. It was extracted from a DEM of the Cartographic Institute of Catalonia with 15 m of spatial resolution (with the ASTER Global DEM at 30 m resolution densified at 15 m to fill the contour zone). Finally, the whole set was densified to 90 m, the final resolution of the climatic maps to be obtained. Latitude (Lat.) is the Euclidean distance taking the 0° parallel (Equator) as a reference. Continentality was modeled by using the Euclidean distance to the Mediterranean coastline (Cont.), as well as the cost distance to the Mediterranean (CostMed) or the Cantabric Sea (CostCant) to account for the influence of mountain barriers. Monthly potential solar radiation (Rad) was extracted from a model proposed by [49] and extensively tested in [50], using the DEM and Sun position coordinates. The Topographic Wetness Index (TWI) [51] is the result of a function between the slope and the top-up contribution area. Although it was designed for hydrological applications, this index can be used as an indicator of the accumulation of cold air masses [52].

3.3. Satellite Land Surface Temperature

Operational Land Surface Temperature (LST) satellite products from MODIS, ATSR-2 and AATSR were considered in this study. They were derived by means of the split-window (SW) method that uses two channels within the 10.5–12.5 μm atmospheric window [53,54]. The main advantage of this method is that it does not require an accurate description of the atmosphere (in the form of vertical profiles of temperature and water vapor, ideally obtained from local, concurrent, radiosonde data) nor radiative transfer calculations based on these profiles. Initially created to estimate sea surface temperatures, the split-window technique was extended to land surfaces by accounting for the effects of surface emissivity (e.g., [55–57]). LST algorithms explicitly include a dependence on the surface emissivity in the channels considered, or alternatively different coefficient sets are provided for each land cover type. In any case, the characteristics of the surface must be well known (via the emissivity, or via the class and amount of vegetation cover) to obtain the LST, which is the main drawback of LST retrieval algorithms.

3.3.1. MODIS Data

The MODIS LST is derived from two thermal infrared band channels, 31 (10.78–11.28 μm) and 32 (11.77–12.27 μm). The atmospheric effects are corrected using the split-window algorithm [56] considering that the signal difference in the two thermal infrared bands is caused by differential absorption of radiation in the atmosphere [58]. The algorithm also corrects for emissivity effects, assuming they are known in each 1 km^2 pixel, using prior knowledge of the land cover type classification [59,60] based on the MODIS Land Cover product (MOD12C1). The MODIS sensor is onboard the Terra and Aqua spacecrafts, which acquire data both during the day and night (see the detailed time of acquisition of the images of this study in Table 2).

The latest MODIS LST version, C6, is a higher quality product than previous versions [61]. This product aims to retrieve LST with an error lower than 1 °C (±0.7 °C standard deviation) in the range of −10 to 50 °C, assuming that surface emissivity is known [59,62]. Validation of the LST algorithm showed errors lower than 1 °C over homogeneous surfaces such as water, crop and grassland surfaces [62,63]. Detailed validation and major refinements implemented in the C6 MODIS LST product are given in [64].

In the present work, MODIS LST products onboard the Terra (MOD11B3) and Aqua (MYD11B3) spacecraft were considered [65]. Their nominal spatial resolution is approximately 5568 m and the products include the associated quality indicator layers. Each LST pixel value is a simple average of all the corresponding valid values in the MOD11B1 or MYD11B1 daily product collected during the month period. To include them in the regression models, images were adapted to 90 m spatial resolution by

means of bilinear interpolation (or the nearest neighbor, in the case of quality layers). From now on, we will refer to products "MODd" or "MODn", and "MYDd" or "MYDn", where d and n refer to the daytime and nighttime products, and MOD and MYD to the Terra and Aqua products, respectively.

Table 2. Local time interval (and average local time) of acquisition of satellite images after considering all the images and pixels of the study area.

Product	Daytime	Nighttime
MOD11B3	10:12–12:00 (11:11)	21:20–23:00 (21:59)
MYD11B3	12:24–13:36 (13:08)	01:24–02:36 (2:04)
ATCDR	10:11–10:59 (10:26)	21:08–22:01 (21:24)

3.3.2. ATSR Data

The AATSR and ATSR-2 LST products are based on the split-window method [66] using the nadir view brightness temperatures at 11 μm and 12 μm. The algorithm expresses the LST as a linear combination of the brightness temperatures depending on the land cover type, the fractional vegetation cover and the precipitable water. It should be noted that land surface emissivity is implicitly handled within the retrieval coefficients dependent on the fractional vegetation. The regression coefficients can be implemented as a look-up table [66] and be updated in a routine manner; the method considers 13 land cover classes or biomes, covering from desert conditions to pine forests.

In this study, we used the ATSR LST Climate Data Record (CDR) Level-3 data, made available through the GlobTemperature Data Portal [67] and generated through the ESA DUE GlobTemperature Project with the support of the UK National Centre for Earth Observation (NCEO) [68]. These data are from the ATSR-2 onboard ERS-2 (from June 1995 to July 2002 inclusive) or from AATSR onboard Envisat (from August 2002 to March 2012), with a spatial resolution of about 0.05°. This prioritizes ATSR-2 data during the commissioning period of AATSR. Moreover, only full months of data were processed.

This product, hereafter called "ATCDRd" or "ATCDRn" for referring to the day or nighttime product respectively (see the detailed time of acquisition of the images of this study in Table 2), is constructed from the data in the Level-2 products (or fitted Level-2 data from the overlap analysis). It is made by mapping the Level-2 pixels onto equal-angle grids, and averaging the LST values—separately for day and night—of overlapping pixels in each grid using the percentage of overlapping area as weight. The input Level-2 products have been validated both within the framework of GlobTemperature and externally. For example, the AATSR LST datasets have been validated against several permanent stations of the Atmospheric Radiation Measurement (ARM) network. These show a bias lower than ±1.0 K with RMSE between 1.6 K and 2.2 K for daytime retrievals, and a bias lower than ±1.0 K with RMSE between 1.1 K and 1.6 K for nighttime retrievals depending on the surface [69]. The product includes the associated LST uncertainty for each grid cell, derived by adding in quadrature the components of the LST uncertainty budget (i.e., random, locally-correlated, systematic).

4. Methodology

4.1. Including LST in the Air Temperature Interpolation Scheme

Although there are different spatial interpolation techniques, we opted to apply a methodology based on multiple linear regression analysis combined with the spatial interpolation of residual errors using inverse distance weighting [12,32,70]. This interpolator offers the possibility of incorporating new geographic variables. In addition, this method has provided better results than other methodologies, at least in the case of T_{air} modeling [32]. The indicated methodology has been applied to produce the Digital Climatic Atlas of the Iberian Peninsula, which includes mean, minimum and maximum monthly and annual temperature layers; obtaining a RMSE of less than 1 °C in all months [33].

Multiple linear regression provides a predictive model of the climatic variable (T_{air}) using the variables that influence the climate of the zone (in our case, the LST has been added to the classic

geographic predictors based on topography and distance surfaces). The result is a potential map obtained from the equation for fitting the regression that explains the general behavior of the climate. Once this potential mapping is available, it is possible to interpolate the residuals of the regression itself to obtain the potential surface closer to the observed data, and therefore, in general, for all the mapped territory. In other words, the use of unexplained variance from the regression model allows, once it is combined with the potential map, to obtain maps that are as realistic as possible. The residuals (difference between the observed value in the meteorological stations and the value predicted by the regression model) show local aspects of the climate not explained by the variables used in the regression or, in other words, they show how distinct the climate is at each point with respect to the general model.

Several reliability indexes were used to describe the thematic quality of each map, using a leave-one-out cross-validation procedure to compare the predicted and observed values from the meteorological stations.

In this study, to analyze the importance of using LST in T_{air} modeling, we used a combined model that includes both geographic and a remote sensing predictor (the LST) in the multiple regression analysis. Moreover, to quantify the improvement resulting from using LST, a multiple regression analysis was also carried out using only geographic variables. In addition, to analyze the implications of model complexity for the T_{air} estimate, two different sets of independent variables were employed to run the model: a first set that only included Alt., Rad., Lat., Cont. and LST as predictors (hereafter called the "simple" model); and a second set that also included TWI, CostMed and CostCant (hereafter called the "complex" model).

4.2. Segmentation Based on Land Cover and Orographic Complexity

To analyze the performance of the model in relation to certain land features that could be relevant, the study area was segmented based on land cover and orographic complexity (see Figure 1).

The study area was segmented into three main land cover categories: *Forests*, *Agricultural and livestock*, and *Urban areas*. This was carried out with version 4 of the Land Cover Map of Catalonia [71], which has 2 m spatial resolution and 25 categories (Level 2). Stations were then classified into categories by considering the mode within a radius of 500 m around each meteorological station. Depending on the month and year, a set of 33 to 38 stations were classified as *Forests*, 99 to 110 as *Agricultural and livestock*, and 44 to 59 as *Urban areas*.

Three levels of orographic complexity of the territory were considered based on the standard deviation of the altitude within a radius of 10 km around each meteorological station. Stations were then classified as *Flat lands* (deviation <150 m), *Middle grounds* (between 150 and 250 m) or *Rugged lands* (>250 m), which included sets of 120–131, 33–46, and 26–34 meteorological stations, respectively.

4.3. Analysis of LST Spatial Scale

The remote sensing LST products used in this study have a spatial resolution of around 6 km, while the regression models were applied to a spatial resolution of 90 m. The spatial scale of LST data was changed accordingly. This change in pixel size is required because the study presented here aims to analyze the improvements gained by including an additional variable in relation to the previous result. Therefore, although some precision was clearly lost by changing the scale of the LST data, it allowed us to achieve our objective. Notwithstanding, two different analyses were carried out to study the possible impact of the original coarse spatial resolution of the LST data on the T_{air} estimates, by segmenting the stations depending on: (1) the heterogeneity in solar radiation; and (2) the heterogeneity in land cover.

As the potential solar radiation did not follow a normal distribution within a ~6 km cell, its variability within a cell was quantified by considering the mean absolute deviation around the median (explained later in Section 4.5). A similar approach was carried out for land cover, but considering the percentage of the mode present within a ~6 km cell. It was then possible to

create one class, named "homogeneous in solar radiation or land cover" (about a third of the stations), that had the lowest deviation values, and one class, named "heterogeneous in solar radiation or land cover" (another third), that had the highest values. Analysis of the performance metrics of each class and their comparison with the performance metrics of models that did not include LST provided some conclusions.

4.4. Weighted Linear Regression Based on LST Quality Bands

To use remote sensing products to derive information about the Earth's surface it is necessary to know well, understand and, if possible, correct or minimize their limitations. In the present work, to eliminate low quality data, LST quality bands provided by the remote sensing products were used in the calibration step to weight the stations included in the model.

Quality information corresponding to each station was assigned by considering the mode (in the case of MODIS) or the mean (in the case of ATCDR, as the uncertainty is given as a continuous variable) within a radius of 10 km (to include at about 3 × 3 pixels) around each meteorological station from quality layers at the resampled spatial resolution (90 m). Then, the stations were weighted following the indications given in Tables 3 and 4 for MODIS and ATCDR data, respectively.

Note that, as observed by [23], MODIS LST uncertainties increase with the MODIS viewing angle, with RMSE being greater than 2 or 3 K for viewing angles $\geq 40^{\circ}$. Thus, they only used MODIS LST measured with angles $<40^{\circ}$ in their study. Nevertheless, this filtering was not necessary in our study because only three images had viewing angles $\geq 40^{\circ}$ and the corresponding stations were already weighted with a small value.

Table 3. Weighting of the meteorological stations according to the quality masks provided by the MOD11B3 and MYD11B3 products. Land surface temperature (LST) quality control (QC) dataset, QC-LST, called as "QC_Mandatory_QA_flag", where QA refers to quality assurance; Emissivity (Emis) quality control dataset, QC-Emis, called as "QC_Emis_error_flag".

QC-LST	QC-Emis	Weighting (%)
1	1,2,3,4	100
3	1	70
3	2	50
3	3	30
3	4	10

Table 4. Weighting of the meteorological stations according to the uncertainty (δ) of the land surface temperature (LST) product from ATCDR.

ATCDR	
δLST (K)	**Weighting (%)**
≤1	100
>1 to ≤1.2	90
>1.2 to ≤1.4	80
>1.4 to ≤1.6	70
>1.6 to ≤1.8	60
>1.8 to ≤2.0	50
>2.0 to ≤2.3	40
>2.3 to ≤2.6	30
>2.6 to ≤3.0	20
>3.0	10

Benali et al. [16] also considered correcting low quality pixels due to non-detected cloud contamination and an error in the optical leak correction that occurred at the end of scan lines and led to anomalous high LST values. However, an accurate examination of our images did not reveal cloud

contamination data or anomalous high LST values, probably because the monthly products considered here only averaged valid values.

4.5. Performance Metrics

Absolute root mean square error ($RMSE_A$) quantifies the scatter between measured (*Meas*) and estimated (*Estim*) values; thus, it can be used to make a quantitative assessment of the accuracy of our estimates:

$$RMSE_A = \sqrt{\frac{1}{N}\sum_{i=1}^{N}(Estim_i - Meas_i)^2} \quad (1)$$

where i refers to each of the N data points (meteorological stations or pixels) analyzed. On the other hand, the coefficient of determination (R^2) provides a measure of how well measures are inferred by the model based on the proportion of total variation of measures explained by the model:

$$R^2 = 1p\frac{\sum_{i=1}^{N}(Meas_i - Estim_i)^2}{\sum_{i=1}^{N}\left(Meas_i - \overline{Meas_i}\right)^2} \quad (2)$$

When the distribution of variable x is not Gaussian, the median ($\hat{x}$) instead of the mean is used as a measure of central tendency, and the mean absolute deviation around the median (σ') is used as a measure of statistical dispersion. σ' was calculated using:

$$\sigma' = \frac{\sum_{i=1}^{N}|x_i - \hat{x}|}{N} \quad (3)$$

For the analysis based on the segmentation of meteorological stations according to their land cover and orographic complexity, or the heterogeneity in potential solar radiation and land cover, only the meteorological stations classified in each class were considered to calculate the metrics. However, all available meteorological stations were considered to analyze the overall performance, as well as to run the model.

5. Results

5.1. Effect of Considering the LST Quality

Performance metrics obtained from weighting linear regression based on LST quality bands were compared to those obtained when no weighting was applied. Detailed results from the analysis (not shown here for brevity), revealed that the impact on the R^2 and $RMSE_A$ was minimal: R^2 remained the same and $RMSE_A$ varied in general by <0.01 K, except for some months with variations up to 0.04 K as maximums when MODIS LST estimates were considered.

This analysis showed it was not necessary to add complexity to the model by weighting linear regressions, with the added bias downplaying relevant stations for the model due to the corresponding quality information of the LST estimates, which is merely indicative. Therefore, the following results did not include the LST quality data.

5.2. Effect of LST Spatial Scale

For this analysis, we used the case with the maximum number of meteorological stations (maximum T_{air} for March 2014). The statistical significance of the selected predictors and performance metrics are summarized in Table 5. A linear correlation analysis between the LST and the analyzed variables (Rad, σ'_{Rad} and the percentage of the mode in land cover) showed that there was no linear dependence between them. Despite this, these characteristics were chosen as they allowed us to analyze the effect of the LST spatial scale, as shown below.

Table 5. Selected model characteristics and performance metrics by considering the meteorological stations classified into two sets (homogeneous and heterogeneous) and regarding their surrounding potential solar radiation (Rad) or land cover attributes. The case analyzed corresponds to the maximum T_{air} observed during March 2014, including or not the LST provided by the daytime MYD11B3 product as an independent variable in the model. LST and Rad denote the standardized regression coefficients, × meaning non-significant ($p > 0.05$). *N*: number of meteorological stations considered.

	N	LST	Rad		$RMSE_A$ (K)		R^2	
			noLST	withLST	noLST	withLST	noLST	withLST
Homo. in Rad	109	0.28	×	×	0.80	0.77	0.55	0.61
Hetero. in Rad	109	0.08	0.069	0.074	0.78	0.78	0.97	0.97
Homo. in land cover	109	0.17	0.037	0.035	1.00	0.97	0.94	0.95
Hetero. in land cover	109	×	0.106	0.106	1.08	1.08	0.91	0.91
All meteo. stations	327	0.10	0.066	0.063	0.80	0.79	0.93	0.94

5.2.1. Analysis in Terms of the Heterogeneity in Solar Radiation

In the analysis shown in Table 5, we observe that when meteorological stations classified as heterogeneous in potential solar radiation (Rad) within a cell of 6 km were considered, the Rad was included in the model as an independent variable. However, it was not the case when meteorological stations that were homogeneous in Rad were considered, which makes sense. Consequently, when models that included LST were considered, the weight of the LST in the regression was smaller in the case of heterogeneous than in homogeneous meteorological stations. A possible reason would be that, in the first case, part of the information was already provided by Rad, while in the second case, the LST provided much more new information. Another reason could be the loss of precision in the LST estimation for heterogeneous meteorological stations due to the change in the LST spatial scale. This effect was also observed in the improvement in the $RMSE_A$ provided by including LST, which was greater for homogeneous (~0.03 K) than for heterogeneous (<0.01 K) stations. Nevertheless, what is important is that, regardless of the accuracy of the LST estimates, the inclusion of this variable was significant (as it was considered as an independent variable by the regression model) and the $RMSE_A$ associated with the T_{air} estimates did not get worse.

The R^2 was much higher when meteorological stations that were heterogeneous in Rad were considered. This is understood to be due to the increase in the dispersion of values, thus providing a better adjustment.

5.2.2. Analysis in Terms of the Heterogeneity in Land Cover

Similarly, we observed that the heterogeneity in land cover downplayed the information provided by the LST to the point that it ceased to be an independent variable in the model (see Table 5). As was the case for Rad, we think that the heterogeneity in land cover unified the LST (it lost precision), and hence, this variable did not provide new information to the regression model. However, the opposite happened in the case of homogeneous meteorological stations. Therefore, it is obvious that an improvement in the spatial resolution of LST would improve the T_{air} estimates. Nevertheless, once again, we observe that, regardless of the accuracy of the LST estimates, the inclusion of this variable was significant (as it was considered as an independent variable by the regression model when all meteorological stations were considered) and the $RMSE_A$ associated with the T_{air} estimates did not get worse (in fact, it decreased by 0.02 K).

5.3. Statistical Comparisons of Model Performance

5.3.1. Models with a Set of Common Meteorological Stations

To compare accuracy metrics more precisely, independently of the months and the number of data points considered, we selected the years with LST data from all sensors (2003–2011) and the 80 meteorological stations common for all cases (see their location in Figure 1a). This allowed us to

study the impact of including LST in the model (Figure 2a) and to decide whether to use it in the research presented here. In addition, it permitted us to examine whether the daytime or nighttime LST product was the most appropriate for estimating maximum or minimum T_{air} (Figure 2b), as well as deciding which LST product usually provides the best T_{air} estimates (Figure 3).

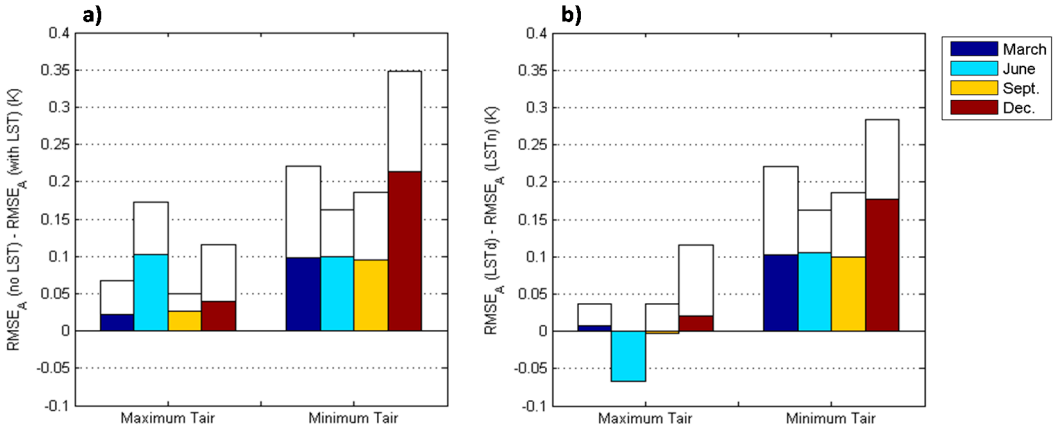

Figure 2. Maximum (white bars) and mean (colored bars) difference in the $RMSE_A$ of T_{air} observed after considering the $RMSE_A$ obtained during the years 2003–2011 in models with 80 common meteorological stations: (**a**) without or with LST; and (**b**) with daytime or nighttime LST (d and n subscripts, respectively).

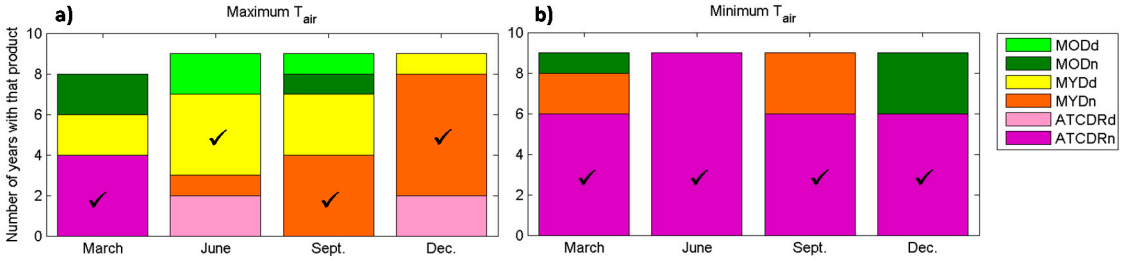

Figure 3. Statistics showing the product providing the best estimates of maximum (**a**) and minimum (**b**) T_{air} (in terms of $RMSE_A$). Results from regressions considering 80 common meteorological stations for the years 2003–2011. For years 2012–2015 without the ATCDR product, LST products providing the best estimates were MYDd for maximum T_{air} in March and June, and MYDn for the other cases.

From the analysis in Figure 2a, we observe that including LST in the models always implied an improvement (in terms of $RMSE_A$ differences) in the T_{air} accuracy, especially for the minimum T_{air} (being up to 0.35 K in December and over 0.15 K in the other months). In the case of maximum T_{air}, the improvement was not as large (<0.12 K), except in June (up to 0.17 K).

In addition, Figure 2b revealed that, except for maximum T_{air} in June, both maximum and minimum T_{air} were clearly better estimated by the nighttime LST products. More specifically, as indicated by Figure 3, the nighttime ATCDR product provided the best proxy for minimum T_{air} for all seasons and for maximum T_{air} in March, while it was MYDn for minimum T_{air} in September and December. Quantitatively, the differences in the $RMSE_A$ given by the other nighttime products were up to 0.10 K, with a mean value of 0.03 K. As an exception, in June the maximum T_{air} was better estimated by the daytime product from Aqua (MYDd), showing $RMSE_A$ differences with the other products of up to 0.11 K.

5.3.2. Analysis Segmented by Land Cover and Orographic Complexity

According to Figure 4, maximum T_{air} estimates were more accurate than minimum T_{air} independently of the land cover or orographic complexity. However, there was no clear pattern between months, while the highest errors for maximum and minimum T_{air} occurred for June and December respectively. Regarding the land cover, Figure 4 shows that meteorological stations classified as *Agricultural and livestock* had the best accuracy in all seasons, with mean $RMSE_A$ values of 0.82 K and 0.98 K for maximum and minimum T_{air} respectively, and maximum $RMSE_A$ values <1 K. *Forests* and *Urban areas* showed similar accuracies for minimum T_{air}, while for maximum T_{air} *Forests* were less accurate than *Urban areas*. In relation to the orographic complexity, there was no clear dependence for the T_{air} accuracy, although we could say that *Rugged lands* showed the lowest and highest accuracies for maximum and minimum T_{air}, respectively.

Figure 5 depicts how the improvement in T_{air} due to including LST was clearly higher for minimum than maximum T_{air} independently of the land cover or orographic complexity. Meteorological stations classified as *Forests* showed the most improvement, with maximum differences between 0.18 and 0.29 K for the maximum T_{air} (in comparison to differences <0.11 K for the other land covers), and between 0.29 K and 0.43 K for the minimum T_{air} (in comparison to differences <0.13 K for *Agricultural and livestock* and <0.28 K for *Urban areas*). Meteorological stations classified as *Rugged lands* had the biggest and clearest improvement for maximum T_{air}, but the smallest improvement (except for December) for minimum T_{air}, for which *Flat lands* showed the best improvement.

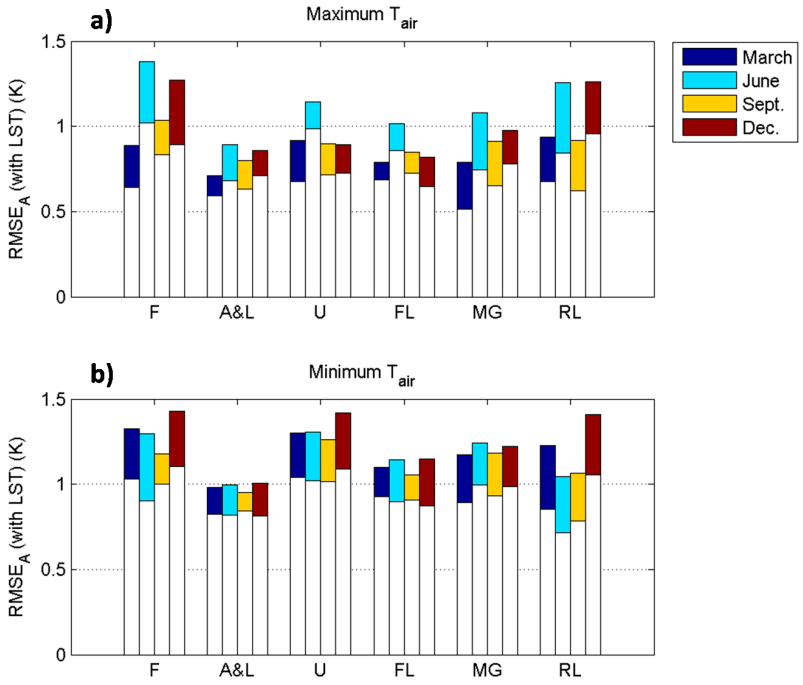

Figure 4. Minimum (white bars) and mean (colored bars) $RMSE_A$ of maximum (**a**) and minimum (**b**) T_{air} obtained by considering models including the LST product providing the best estimates (in terms of $RMSE_A$). Results from regressions for the years 2003–2015 and the following sets of meteorological stations: F: *Forests*; A&L: *Agricultural and livestock*; U: *Urban areas*; FL: *Flat lands*; MG: *Middle grounds*; RL: *Rugged lands*.

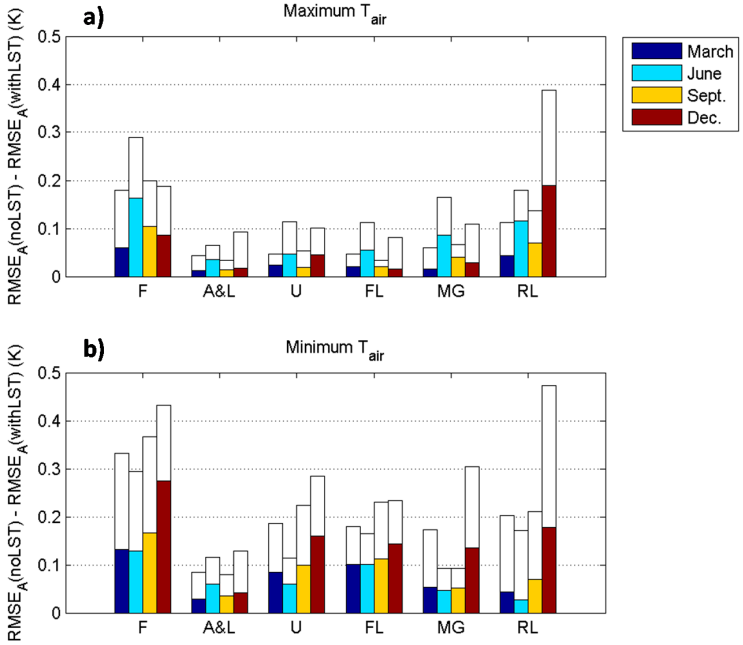

Figure 5. Maximum (white bars) and mean (colored bars) difference in the $RMSE_A$ of maximum (**a**) and minimum (**b**) T_{air} obtained by considering models without LST and models including the LST product providing the best estimates (in terms of $RMSE_A$). Results from regressions for the years 2003–2015 and the following sets of meteorological stations: F: *Forests*; A&L: *Agricultural and livestock*; U: *Urban areas*; FL: *Flat lands*; MG: *Middle grounds*; RL: *Rugged lands*.

5.3.3. Implication of Model Complexity

As shown by the statistics in Figure 6a,b, the accuracy of T_{air} improved ($\Delta RMSE_A > 0$ K) when all considered independent variables were included, while it was more significant for maximum T_{air} (with differences up to 0.17 K, and mean values from 0.06 K to 0.09 K, except in December). However, the improvement for minimum T_{air} was slight (with differences <0.05 K) or even inexistent in some cases. The R^2 decreased with the complexity of the model by up to 0.11 K for maximum T_{air} (Figure 6c), although there was less of a decrease (0.03 K as maximum) for minimum T_{air} (Figure 6d).

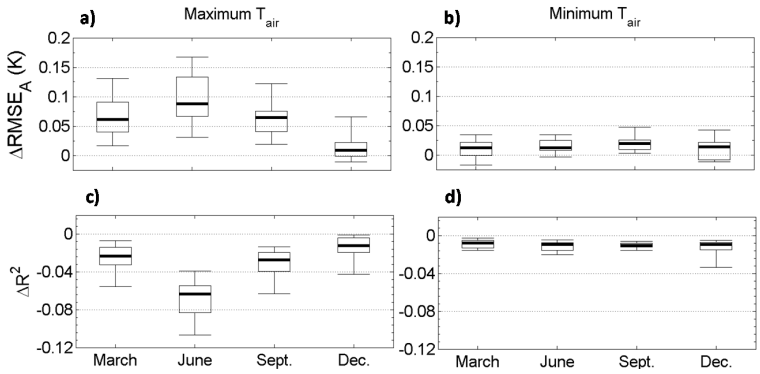

Figure 6. Temporal variation of the difference between the $RMSE_A$ and the R^2 of maximum (**a**,**c**) and minimum (**b**,**d**) T_{air} obtained with the "simple" and the "complex" models. Each boxplot belongs to model results for the years 2003–2015 by considering all meteorological stations and LST estimates from the products indicated in Figure 3. Each boxplot comprises the median (central thick line), the first and the third quartile (inferior and superior edges of the boxes), and the extreme values excluding outliers (inferior and superior whiskers, corresponding to percentiles 0.5% and 99.5% respectively).

5.3.4. Overall Performance

To give an idea of the overall performance achieved with our method, $RMSE_A$ and R^2 value metrics corresponding to all years and months are summarized in Figure 7. To simplify, for these plots the model considered the selected LST products indicated in Figure 3. As already seen in Section 5.3.2, maximum T_{air} had better accuracies than minimum T_{air}, even though in neither case did they exceed 1.6 K. Mean $RMSE_A$ values ranged from 0.8 to 1.1 K for maximum T_{air}, and from 1.1 to 1.2 K for minimum T_{air}. Similarly, the goodness of fit (explained by the R^2), was much better for maximum than minimum T_{air}, especially for some of the warmest months (March, June and September). Mean values varied from 0.90 to 0.95 and from 0.83 to 0.88 for maximum and minimum T_{air}, respectively.

In addition, to test the consistency of the model, we analyzed the linear relationship between the calculated and ground measured T_{air}. As an example, Figure 8 shows the dispersion of values observed for maximum and minimum T_{air}, together with the linear fit and the statistics, which were slightly better for maximum T_{air}. We also carried out a more in-depth analysis that considered the months separately, and segmented by land cover or by orographic complexity. The analysis results (not shown here for brevity) revealed that the performance metrics were practically equivalent to the mean values shown in Figures 4 and 7.

Figure 9 gives evidence of the improvement in accuracy for T_{air} estimates gained by including LST. The improvement was greater for minimum T_{air}, except in June. Differences in mean $RMSE_A$ for maximum T_{air} ranged from 0.015 to 0.06 K, and from 0.05 to 0.12 K for minimum T_{air}. Nevertheless, differences were up to 0.1 K and 0.2 K for maximum and minimum T_{air}, respectively. From the comparison with Figure 6, we observe that including LST as a predictor of minimum T_{air} led to a much larger improvement than that provided by additional geographic data (i.e., TWI, CostMed and CostCant), while its contribution to maximum T_{air} was less important. The regression coefficients of the model (Figure 10) also give evidence of this effect, as for minimum T_{air} the LST variable is the most important one, and for maximum T_{air} its weight is moderate, being the altitude the most relevant parameter. The analysis of results observed by running the model considering only the LST as independent variable (Figure 8c,d) gives again evidence of the improvement provided by such variable. Specifically, LST by itself can provide a high accuracy in minimum T_{air} (1.41 °C) in comparison with results from a model considering all independent variables (1.16 °C), while the achieved accuracy is not so high for minimum T_{air} (2.16 °C vs. 1.01 °C).

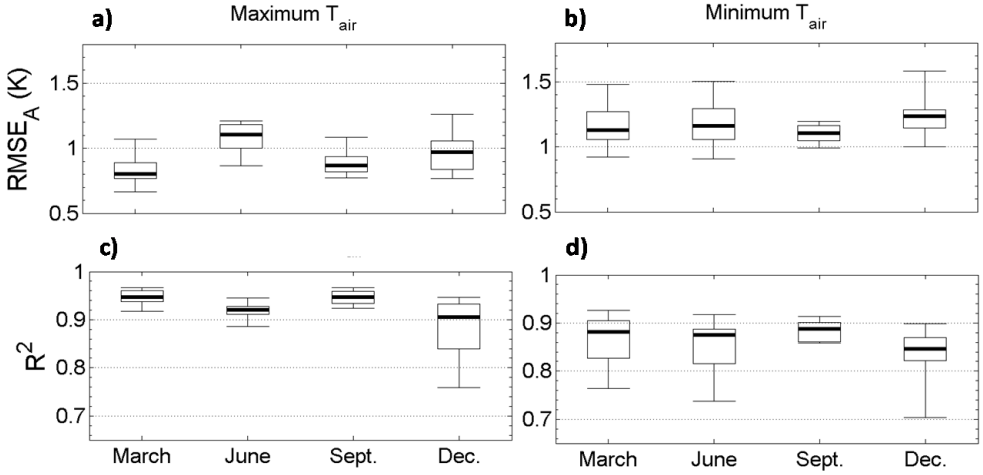

Figure 7. Idem to Figure 6, but corresponding to performance metrics obtained with the "complex" model.

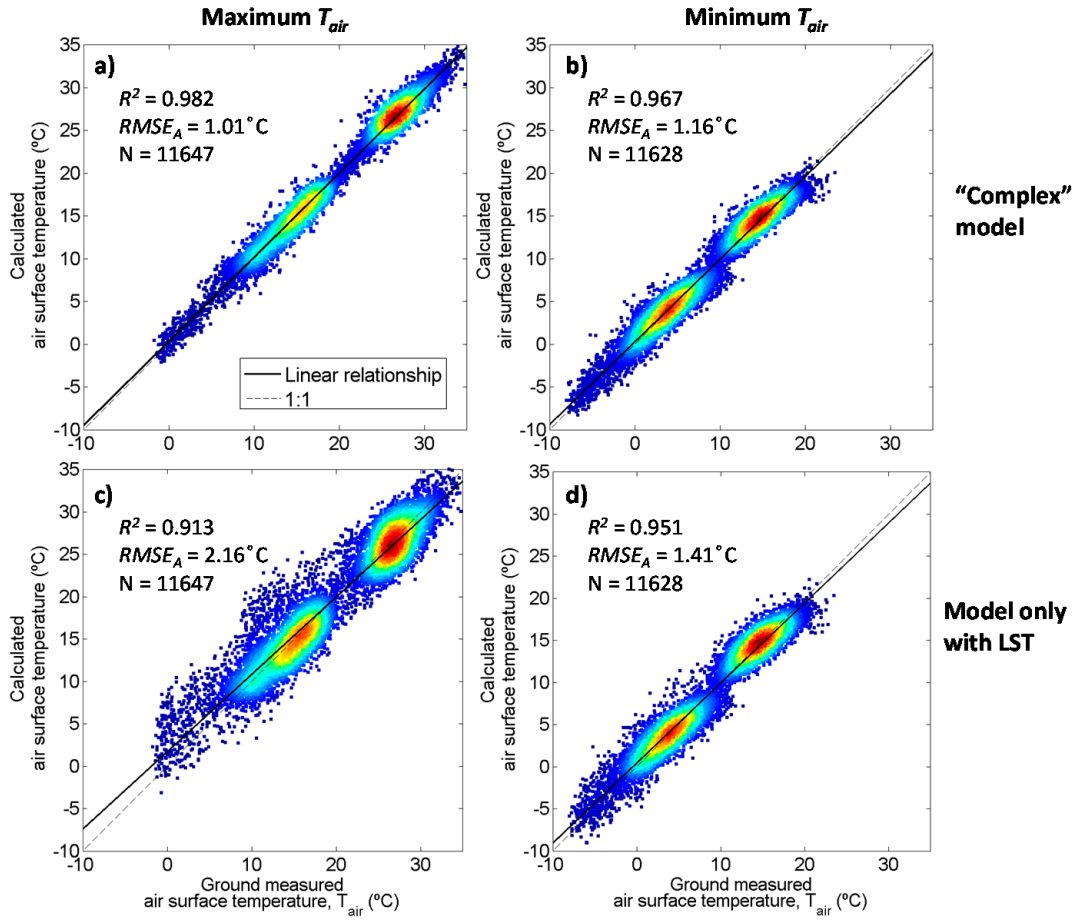

Figure 8. Density scatter plot between calculated T_{air} and ground measured maximum and minimum T_{air}, using data from all years, months and meteorological stations by considering: (**a**,**b**) the "complex" model, which includes all independent variables; and (**c**,**d**) a model considering only the LST as independent variable. This figure corresponds to model results that consider LST estimates from the products indicated as Figure 3. Reddish points indicate high density. N: number of samples.

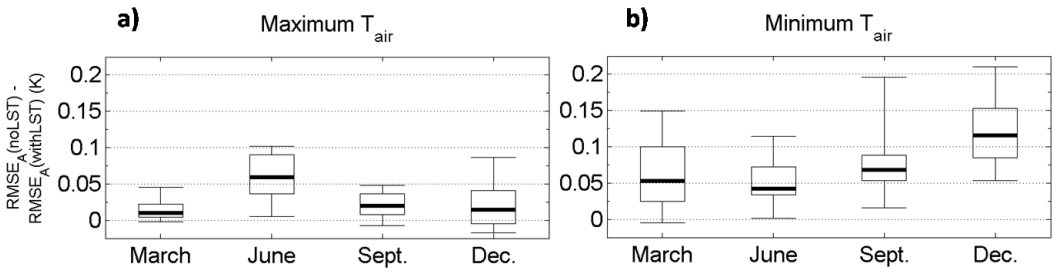

Figure 9. Idem to Figure 6a,b, but corresponding to the differences between performance metrics achieved by models without LST and models with LST.

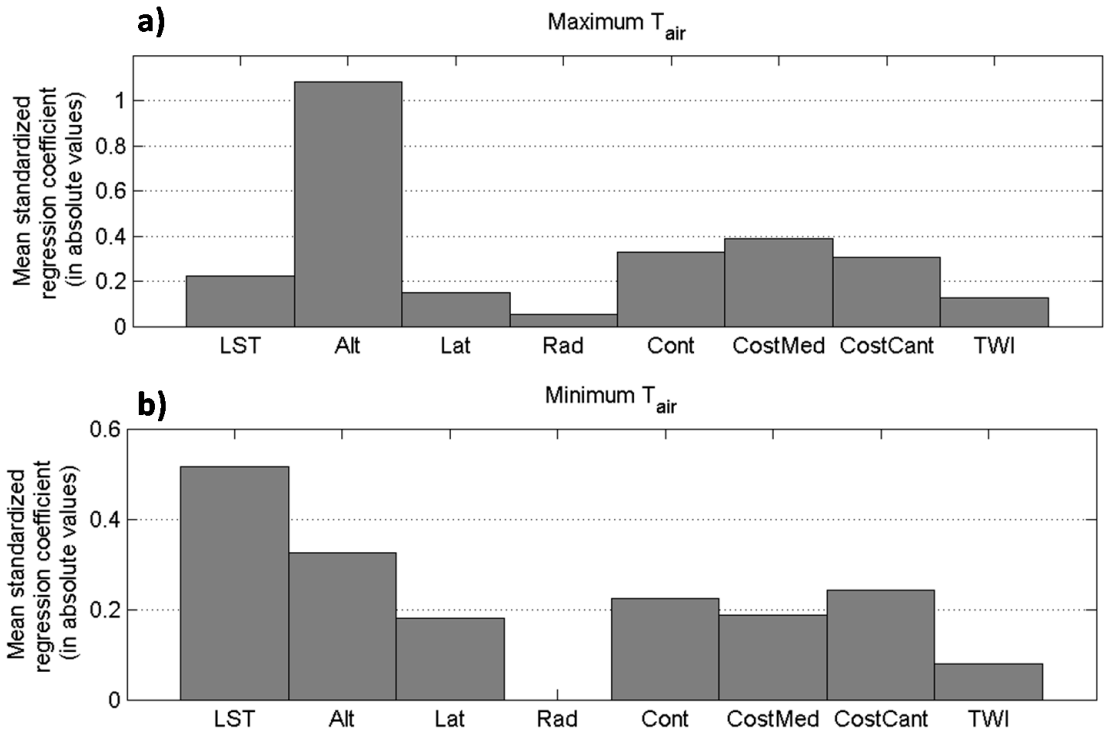

Figure 10. Mean value for the standardized regression coefficients (in absolute values) obtained for the month-to-month maximum (**a**) and minimum (**b**) T_{air} estimates, by considering all years, months, and meteorological stations for models including the LST product indicated in Figure 3. Alt.: altitude; Lat.: latitude; Rad: potential solar radiation; Cont.: continentality; CostMed and CostCant: cost distance to the Mediterranean Sea or Cantabric Sea, respectively; TWI: topographic wetness index.

While all these results only concerned values corresponding to the meteorological stations, Figure 11 depicts the spatial and temporal variation over all the study area during a selected year. Although these maps do not show which model is the best (as there is no comparison with ground measurements), they provide a spatial and temporal quantitative view of the differences between the results of the model that considers LST and the model that does not. These differences were smaller in March and much more pronounced in the other months, especially over high altitude areas in the northwest of Catalonia, which corresponded to *Rugged lands* (see Figure 1b), with absolute differences exceeding 1.2 K. More details are observed in Figure 12, which shows the spatial difference over areas with a dominant land cover. The highest T_{air} differences were observed over *Urban areas* (black and blue pixels in Figure 12c), followed by some *Forest* areas (green pixels in Figure 12c and blue pixels in Figure 12a) and *Agricultural and livestock* regions (cyan pixels in Figure 12c and the different shades of green in Figure 12b).

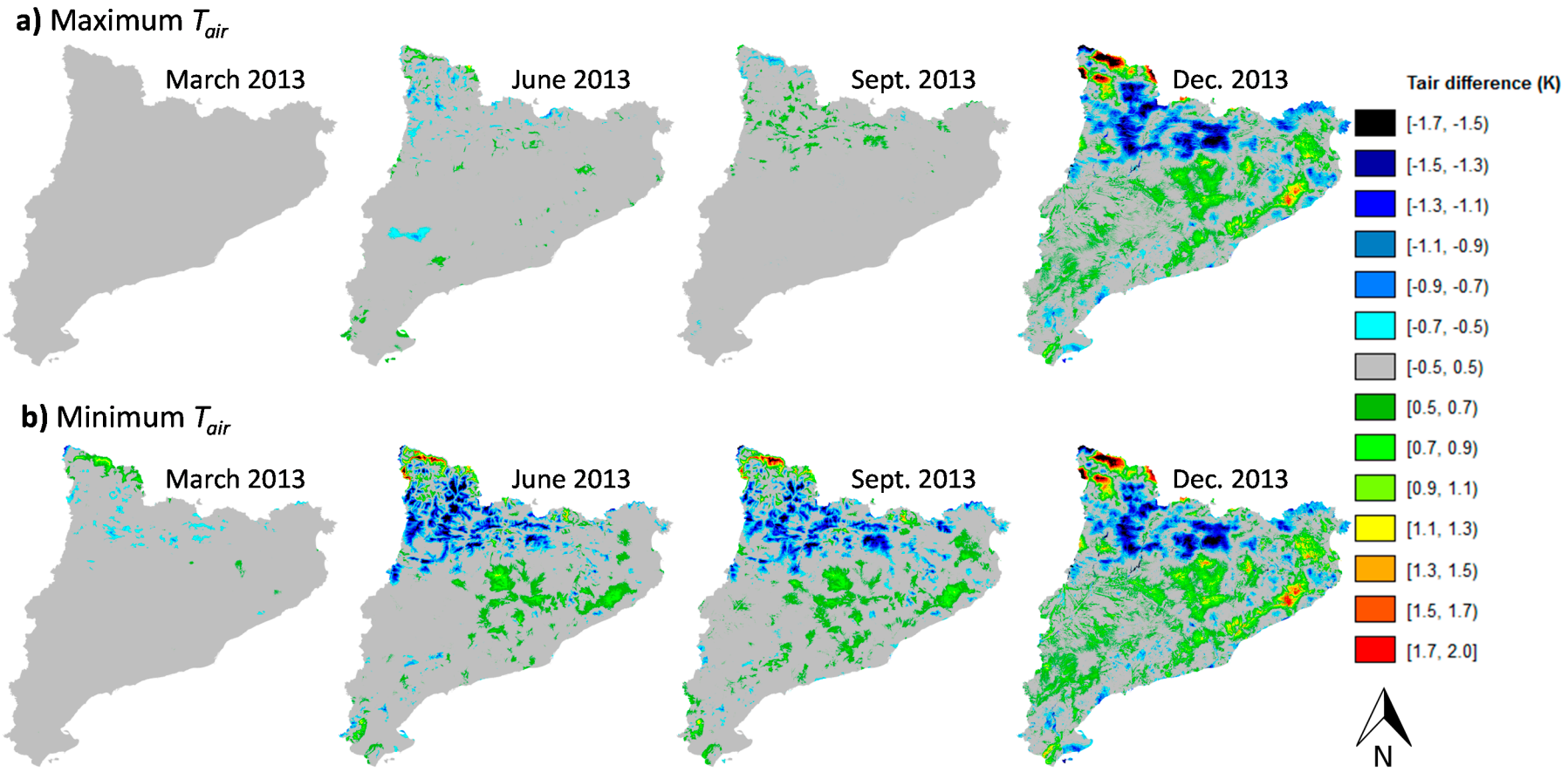

Figure 11. Spatial and temporal variation of the difference in the maximum (**a**) and minimum (**b**) T_{air} estimates provided by models without LST and models with LST: maps were obtained by subtracting T_{air} (with LST) from T_{air} (no LST). This figure corresponds to model results for 2013 over the area of interest and considering all meteorological stations and LST estimates from MYDn, except for maximum T_{air} in March and June, for which MYDd was used instead.

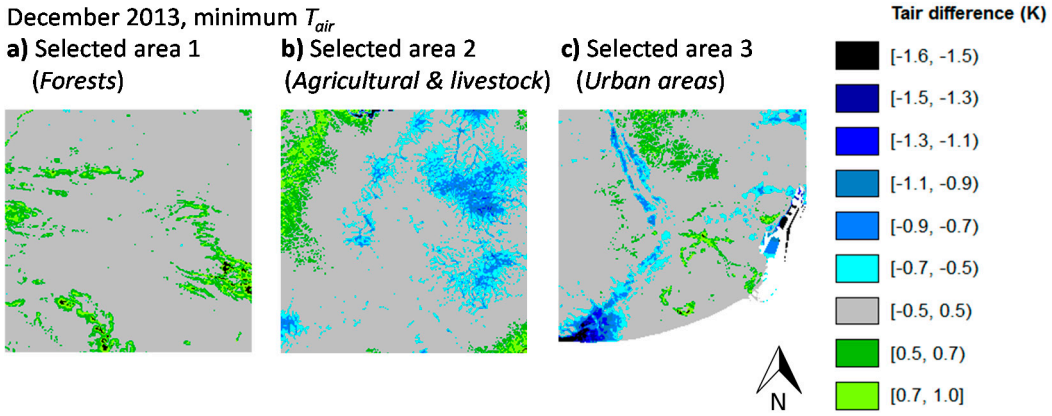

Figure 12. Spatial variation of the difference in the minimum T_{air} estimates provided by models without LST and by models with LST: maps were obtained by subtracting T_{air} (with LST) from T_{air} (no LST). This example corresponds to the model results for December 2013 over three selected areas (**a**–**c**) mainly characterized by a certain land cover (see their location in Figure 1), and considering all meteorological stations and LST estimates from MYDn.

6. Discussion

6.1. Improvements from Including LST

This study shows the strong physical relationship between LST and T_{air} and evidence the potential of using MODIS and ATCDR LST monthly data to estimate month-to-month T_{air} dynamics at a detailed spatial resolution (90 m), despite their rough original spatial resolution (~6 km).

According to [16], daytime and nighttime LST are the most relevant predictors. From comparisons of Figures 6 and 9, we observe that our study is clearly in agreement with these authors for minimum T_{air}, while it is not so evident for maximum T_{air}. Nevertheless, whatever the range of improvement achieved, it is clear that including remotely sensed LST estimates as a predictor in classical T_{air} modeling is positive (Figures 2 and 5).

6.2. Differences between Daytime and Nighttime LST

As observed by different authors [16–20], besides data availability, cloud contamination and angular effects, the time of overpass of the remote sensor has an impact on the accuracy of T_{air} estimates. However, [21] stated that the difference between satellite overpass and the timing of maximum or minimum T_{air} was not critical.

Regarding our considered LST products, MODIS Aqua time of overpass is closer than MODIS Terra and ATCDR to the time of minimum and maximum T_{air} (Table 2). Similarly to [18,19] and contrary to [22], we found that the $RMSE_A$ of T_{air} estimation was higher using MODIS Terra than Aqua, although it should be noted that ATCDR provided the best estimates (due to differences in the accuracy of the products).

Furthermore, it is important to note that, generally, most of the studies [16,18,23] consider nighttime LST data as a covariate to predict minimum T_{air}, and daytime LST data to predict maximum T_{air}. Our research, in agreement with findings by [20,37] over complex terrain and by [19] over the Corn Belt in the U.S., showed that nighttime LST provided a good proxy of minimum T_{air}, while models with daytime LST had the lowest accuracy. However, in agreement with findings by [17] and [19] and following recommendations by [20], our study also showed that nighttime LST provided a good proxy of maximum T_{air}. Interestingly, by combining both daytime and nighttime LST data, it is possible to improve the accuracy of maximum T_{air}, while no significant improvement in accuracy is found for minimum T_{air} estimates [19], indicating that daytime LST is not relevant for estimating minimum T_{air}. In addition, as observed by [16], combining MODIS Terra and Aqua data also has great potential for

T_{air} estimation. Therefore, future research could focus on combining data sources, as well as daytime and nighttime LST estimates.

6.3. Temporal and Spatial Patterns

The derived datasets were representative of T_{air} dynamics for the whole study region, but also for regions characterized by a predominant land cover and by orographic complexity. Our analysis showed that model performance did not follow a clear seasonal pattern for either maximum or minimum T_{air}, while there were significant differences between accuracies for maximum T_{air} but not for minimum T_{air}. Benali et al. [16] and Zeng et al. [19] observed higher accuracy for daily T_{air} estimates in summer, which they attributed to the prevalence of clear skies. On the contrary, we observed the lowest accuracy for maximum month-to-month T_{air} estimates in summer (June), followed by those in winter (December), and the highest accuracy in spring (March).

From an analysis at station level, Benali et al. [16] and Zeng et al. [19] found that, in general, the meteorological stations located in forests had a better performance than those in crop and urban areas, with the lowest performance for stations in urban areas. From the analysis of Figures 11 and 12, we observed that our performances followed the same pattern. Nevertheless, it is worth mentioning that the statistics in Figure 5 are probably not strictly comparable between them, except for the seasonal variation within each class, due to the different number of stations classified in each class.

Similarly, the analysis results in Figures 11 and 12 showed that the month-to-month T_{air} accuracy improved with the decrease in terrain roughness, in accordance with the findings by [19,20]. Further, in agreement with [18], we also observed high errors in minimum T_{air} over water surfaces due to the inertia of water, which may lead to an underestimation or an overestimation of minimum T_{air} according to the temperature of the previous months, respectively cooler or warmer than the present [18].

7. Conclusions

The good results of this study can be considered operational given the feasibility of the models employed (linear dependence on predictors that are already easily available), the robustness of the leave-one-out cross-validation procedure and the improvement in accuracy achieved compared to classical T_{air} modeling results.

The results were within or above the accuracies reported in the literature considering the methodologies for T_{air} estimation based on remote sensing LST. The model had a general tendency to present lower performance but higher improvements for minimum T_{air} in comparison with maximum T_{air}. This is especially relevant as month-to-month minimum T_{air} prediction using only GIS-based geographical variables often provides unexpected results. Quantitatively, on the one hand, the models estimated maximum and minimum month-to-month T_{air} with mean $RMSE_A$ within 0.8–1.1 K and 1.1–1.2 K, respectively, and mean R^2 within 0.90–0.95 and 0.83–0.88, respectively. On the other hand, the inclusion of LST into the models implied an accuracy improvement up to 0.35 K in relation to classical T_{air} modeling on December and beyond 0.15 K on the other months for minimum T_{air}, while for maximum T_{air} it was not as important (<0.12 K), except on June (up to 0.17 K). The improvement was higher over *Forests* and *Rugged lands*. Results are really encouraging as there are generally few meteorological stations in zones with these characteristics, clearly showing the usefulness of remote sensing to improve information for areas that are difficult to access or simply with a poor availability of conventional meteorological data. Such improvement was thanks to the LST, which provides additional information in relation to phenomena as the thermal inversion, not reflected so far, or not enough, by geographic variables or in situ measurements, probably due to the few meteorological stations located on rugged lands.

Although it might seem that the improvement was not very high, it is important to note that the improvement provided by the new model was clear and robust and that can be applied routinely. Currently, within the study of trends in the context of climate change, such improvement is relevant, as spatial and temporal finer resolutions are often required and, of course, higher accuracies are needed.

Moreover, this is in line with the increase of operational LST products developed by some Spatial Agencies. A wide scope of applications can benefit from the improved remote sensing based T_{air} estimations presented in this work. Further, as an added value, we would like to mention that this work will imply the update and improvement of the "Digital Climate Atlas of Catalonia" developed by the Autonomous University of Barcelona and available online [72].

Acknowledgments: This research was funded by the Spanish Ministry of Economy and Competitiveness through the project ACAPI (CGL2015-69888-P MINECO/FEDER) and the post-doctoral contract "Juan de la Cierva" granted to M. Mira, as well as by the Government of Catalonia (2014 SGR1491). X. Pons is a recipient of an ICREA Academia Excellence in Research grant 2016–2020. We are grateful to the MODIS mission scientists and associated NASA personnel for the production of the data used in this research effort. We acknowledge the ESA DUE GlobTemperature Project and the UK National Centre for Earth Observation (NCEO) for the generation of the ATSR LST Climate Data Record (CDR) Level-3 data. Meteorological data were provided by AEMET (Spanish National Meteorological Agency) and SMC (Catalan Meteorological Service).

Author Contributions: M.N. and M.B. prepared the meteorological stations data and other geographic data. M.M. prepared the remote sensing data, implemented the code (with the support of M.B.), produced the results and wrote the draft of the manuscript. X.P. and L.P. wrote the code to fit and generate climate surfaces. M.N., M.B., L.P. and X.P. contributed to the discussion of the results, providing valuable insights, and reviewed the manuscript.

Conflicts of Interest: The authors declare no conflict of interest.

References

1. Wylie, R.G.; Lalas, T. *Measurement of Temperature and Humidity*; Technical Note No. 194, WMO-No. 759; World Meteorological Organization (WMO): Geneva, Switzerland, 1992.
2. Idso, S.B. A set of equations for full spectrum and 8 μm to 14 μm and 10.5 μm to 12.5 μm thermal radiation from cloudless skies. *Water Resour. Res.* **1981**, *17*, 295–304. [CrossRef]
3. Kustas, W.P.; Norman, J.M. Use of remote sensing for evapotranspiration monitoring over land surfaces. *Hydrol. Sci. J.* **1996**, *41*, 495–516. [CrossRef]
4. Prihodko, L.; Goward, S.N. Estimation of air temperature from remotely sensed surface observations. *Remote Sens. Environ.* **1997**, *60*, 335–346. [CrossRef]
5. Bastiaanssen, W.G.M.; Menenti, M.; Feddes, R.A.; Holtslag, A.A.M. A remote sensing surface energy balance algorithm for land (SEBAL)-1. Formulation. *J. Hydrol.* **1998**, *213*, 198–212. [CrossRef]
6. Kustas, W.P.; French, A.N.; Hatfield, J.L.; Jackson, T.J.; Moran, M.S.; Rango, A.; Ritchie, J.C.; Schmugge, T.J. Remote sensing research in hydrometeorology. *Photogramm. Eng. Remote Sens.* **2003**, *69*, 631–646. [CrossRef]
7. Kuhn, K.G.; Campbell-Lendrum, D.H.; Davies, C.R. A continental risk map for malaria mosquito (Diptera: Culicidae) vectors in Europe. *J. Med. Entomol.* **2002**, *39*, 621–630. [CrossRef] [PubMed]
8. Chow, V.T.; Maidment, D.R.; Mays, L.W. *Applied Hydrology*; Mcgraw-Hill: Singapore, 1998.
9. Prince, S.D.; Goward, S.N. Global primary production: A remote sensing approach. *J. Biogeogr.* **1995**, *22*, 815–835. [CrossRef]
10. IPCC. Climate change 2007: The physical science basis. In *Contribution of Working Group I to the Fourth Assessment Report of the Intergovernmental Panel on Climate Change*; Solomon, S., Qin, D., Manning, M., Chen, Z., Marquis, M., Averyt, K.B., Tignor, M., Miller, H.L., Eds.; Cambridge University Press: Cambridge, UK, 2007.
11. Vicente-Serrano, S.M.; Heredia-Laclaustra, A. Nao influence on NDVI trends in the Iberian Peninsula (1982–2000). *Int. J. Remote Sens.* **2004**, *25*, 2871–2879. [CrossRef]
12. Sun, Y.J.; Wang, J.F.; Zhang, R.H.; Gillies, R.R.; Xue, Y.; Bo, Y.C. Air temperature retrieval from remote sensing data based on thermodynamics. *Theor. Appl. Climatol.* **2005**, *80*, 37–48. [CrossRef]
13. Cristóbal, J.; Ninyerola, M.; Pons, X. Modeling air temperature through a combination of remote sensing and gis data. *J. Geophys. Res. Atmos.* **2008**, *113*. [CrossRef]
14. Hengl, T.; Heuvelink, G.B.M.; Tadic, M.P.; Pebesma, E.J. Spatio-temporal prediction of daily temperatures using time-series of MODIS LST images. *Theor. Appl. Climatol.* **2012**, *107*, 265–277. [CrossRef]
15. Yang, Y.; Cai, W.; Yang, J. Evaluation of MODIS land surface temperature data to estimate near-surface air temperature in northeast China. *Remote Sens.* **2017**, *9*, 410. [CrossRef]
16. Benali, A.; Carvalho, A.C.; Nunes, J.P.; Carvalhais, N.; Santos, A. Estimating air surface temperature in Portugal using MODIS LST data. *Remote Sens. Environ.* **2012**, *124*, 108–121. [CrossRef]

17. Xu, Y.M.; Knudby, A.; Ho, H.C. Estimating daily maximum air temperature from MODIS in British Columbia, Canada. *Int. J. Remote Sens.* **2014**, *35*, 8108–8121. [CrossRef]
18. Vancutsem, C.; Ceccato, P.; Dinku, T.; Connor, S.J. Evaluation of MODIS land surface temperature data to estimate air temperature in different ecosystems over Africa. *Remote Sens. Environ.* **2010**, *114*, 449–465. [CrossRef]
19. Zeng, L.L.; Wardlow, B.D.; Tadesse, T.; Shan, J.; Hayes, M.J.; Li, D.R.; Xiang, D.X. Estimation of daily air temperature based on MODIS land surface temperature products over the corn belt in the US. *Remote Sens.* **2015**, *7*, 951–970. [CrossRef]
20. Mutiibwa, D.; Strachan, S.; Albright, T. Land surface temperature and surface air temperature in complex terrain. *IEEE J. Sel. Top. Appl. Earth Obs. Remote Sens.* **2015**, *8*, 4762–4774. [CrossRef]
21. Mostovoy, G.V.; King, R.L.; Reddy, K.R.; Kakani, V.G.; Filippova, M.G. Statistical estimation of daily maximum and minimum air temperatures from MODIS LST data over the state of Mississippi. *Geosci. Remote Sens.* **2006**, *43*, 78–110. [CrossRef]
22. Zhu, W.B.; Lu, A.F.; Jia, S.F. Estimation of daily maximum and minimum air temperature using MODIS land surface temperature products. *Remote Sens. Environ.* **2013**, *130*, 62–73. [CrossRef]
23. Niclòs, R.; Valiente, J.A.; Barberà, M.J.; Caselles, V. Land surface air temperature retrieval from EOS-MODIS images. *IEEE Geosci. Remote Sens. Lett.* **2014**, *11*, 1380–1384. [CrossRef]
24. Mira, M.; Olioso, A.; Gallego-Elvira, B.; Courault, D.; Garrigues, S.; Marloie, O.; Hagolle, O.; Guillevic, P.; Boulet, G. Uncertainty assessment of surface net radiation derived from Landsat images. *Remote Sens. Environ.* **2016**, *175*, 251–270. [CrossRef]
25. Vazquez, D.P.; Reyes, F.J.O.; Arboledas, L.A. A comparative study of algorithms for estimating land surface temperature from AVHRR data. *Remote Sens. Environ.* **1997**, *62*, 215–222. [CrossRef]
26. Zaksek, K.; Schroedter-Homscheidt, M. Parameterization of air temperature in high temporal and spatial resolution from a combination of the SEVIRI and MODIS instruments. *ISPRS J. Photogramm. Remote Sens.* **2009**, *64*, 414–421. [CrossRef]
27. Vogt, J.V.; Viau, A.A.; Paquet, F. Mapping regional air temperature fields using satellite-derived surface skin temperatures. *Int. J. Climatol.* **1997**, *17*, 1559–1579. [CrossRef]
28. Cresswell, M.P.; Morse, A.P.; Thomson, M.C.; Connor, S.J. Estimating surface air temperatures, from Meteosat land surface temperatures, using an empirical solar zenith angle model. *Int. J. Remote Sens.* **1999**, *20*, 1125–1132. [CrossRef]
29. Jang, J.D.; Viau, A.A.; Anctil, F. Neural network estimation of air temperatures from AVHRR data. *Int. J. Remote Sens.* **2004**, *25*, 4541–4554. [CrossRef]
30. Czajkowski, K.P.; Goward, S.N.; Stadler, S.J.; Walz, A. Thermal remote sensing of near surface environmental variables: Application over the Oklahoma Mesonet. *Profr. Geogr.* **2000**, *52*, 345–357. [CrossRef]
31. Meteotest. Meteonorm Handbook Part II: Theory. 2010. Available online: www.meteonorm.com/images/uploads/downloads/mn72_theory7.2.pdf (accessed on 19 September 2017).
32. Ninyerola, M.; Pons, X.; Roure, J.M. A methodological approach of climatological modelling of air temperature and precipitation through GIS techniques. *Int. J. Climatol.* **2000**, *20*, 1823–1841. [CrossRef]
33. Ninyerola, M.; Pons, X.; Roure, J.M. Objective air temperature mapping for the Iberian Peninsula using spatial interpolation and GIS. *Int. J. Climatol.* **2007**, *27*, 1231–1242. [CrossRef]
34. Ninyerola, M.; Pons, X.; Roure, J.M. Monthly precipitation mapping of the Iberian Peninsula using spatial interpolation tools implemented in a geographic information system. *Theor. Appl. Climatol.* **2007**, *89*, 195–209. [CrossRef]
35. Stisen, S.; Sandholt, I.; Norgaard, A.; Fensholt, R.; Eklundh, L. Estimation of diurnal air temperature using MSG Seviri data in West Africa. *Remote Sens. Environ.* **2007**, *110*, 262–274. [CrossRef]
36. Meyer, H.; Katurji, M.; Appelhans, T.; Muller, M.U.; Nauss, T.; Roudier, P.; Zawar-Reza, P. Mapping daily air temperature for Antarctica based on MODIS LST. *Remote Sens.* **2016**, *8*, 732. [CrossRef]
37. Noi, P.; Kappas, M.; Degener, J. Estimating daily maximum and minimum land air surface temperature using MODIS land surface temperature data and ground truth data in northern Vietnam. *Remote Sens.* **2016**, *8*, 1002. [CrossRef]
38. Cai, Y.; Chen, G.; Wang, Y.; Yang, L. Impacts of land cover and seasonal variation on maximum air temperature estimation using MODIS imagery. *Remote Sens.* **2017**, *9*, 233. [CrossRef]

39. Huang, R.; Zhang, C.; Huang, J.; Zhu, D.; Wang, L.; Liu, J. Mapping of daily mean air temperature in agricultural regions using daytime and nighttime land surface temperatures derived fromTerra and Aqua MODIS data. *Remote Sens.* **2015**, *7*, 8728–8756. [CrossRef]
40. Chen, F.G.; Liu, Y.; Liu, Q.; Qin, F. A statistical method based on remote sensing for the estimation of air temperature in China. *Int. J. Climatol.* **2015**, *35*, 2131–2143. [CrossRef]
41. Sahin, M. Modelling of air temperature using remote sensing and artificial neural network in Turkey. *Adv. Space Res.* **2012**, *50*, 973–985. [CrossRef]
42. Yao, Y.H.; Zhang, B.P. MODIS-based air temperature estimation in the southeastern Tibetan Plateau and neighboring areas. *J. Geogr. Sci.* **2012**, *22*, 152–166. [CrossRef]
43. Shen, L.; Guo, X.L.; Xiao, K. Spatiotemporally characterizing urban temperatures based on remote sensing and GIS analysis: A case study in the city of Saskatoon (SK, Canada). *Open Geosci.* **2015**, *7*, 27–39. [CrossRef]
44. Clavero, P.; Martín-Vide, J.; Raso-Nadal, J. *Atles Climàtic de Catalunya. Termopluviometria i Radiació Solar*; Servei Meteorològic de Catalunya, Generalitat de Catalunya (Departament de Política Territorrial i Obres Públiques), Institut Cartogràfic de Catalunya and Departament de Medi Ambient: Barcelona, Spain, 1996.
45. Folch i Guillèn, R. *La Vegetació dels Països Catalans*, 2nd ed.; Institució Catalana D'història Natural, Memoria Núm. 10; Editorial Ketres: Barcelona, Spain, 1986.
46. Ibáñez, J.; Burriel, J. Mcsc: A High-Resolution Thematic Digital Cartography. In Proceedings of the 5th European Congress on Regional Geoscientific Cartography and Information Systems, Barcelona, Spain, 13–16 June 2006; pp. 278–280.
47. Spanish National Meteorological Agency (Aemet). Available online: http://www.aemet.es (accessed on 19 September 2017).
48. Catalan Meteorological Service (SMC). Available online: http://www.meteo.cat (accessed on 19 September 2017).
49. Pons, X. Estimación de la radiación solar a partir de modelos digitales de elevaciones. Propuesta metodológica. In *VII Coloquio de Geografía Cuantitativa, Sistemas de Información Geográfica y Teledetección*; Juaristi, J., Moro, I., Eds.; Association of Spanish Geographers: Vitoria-Gasteiz, Spain, 1996; pp. 87–97.
50. Pons, X.; Ninyerola, M. Mapping a topographic global solar radiation model implemented in a GIS and refined with ground data. *Int. J. Climatol.* **2008**, *28*, 1821–1834. [CrossRef]
51. Böhner, J.; Köthe, R.; Conrad, O.; Gross, J.; Ringeler, A.; Selige, T. Soil regionalisation by means of terrain analysis and process parameterisation. In *Soil Classification 2001*; Micheli, E., Nachtergaele, F., Montanarella, L., Eds.; European Soil Bureau, Research Report No. 7, EUR 20398 EN; European Commission: Luxembourg, 2002; pp. 213–222.
52. Pypker, T.G.; Barnard, H.R.; Hauck, M.; Sulzman, E.W.; Unsworth, M.H.; Mix, A.C.; Kennedy, A.M.; Bond, B.J. Can carbon isotopes be used to predict watershed-scale transpiration? *Water Resour. Res.* **2009**, *45*. [CrossRef]
53. Prabhakara, C.; Dalu, G.; Kunde, V.G. Estimation of sea surface temperature from remote sensing in 11 to 13 μm window region. *J. Geophys. Res.* **1974**, *79*, 5039–5044. [CrossRef]
54. Deschamps, P.Y.; Phulpin, T. Atmospheric correction of infrared measurements of sea surface temperature using channels at 3.7, 11 and 12 μm. *Bound. Layer Meteorol.* **1980**, *18*, 131–143. [CrossRef]
55. Becker, F.; Li, Z.L. Towards a local split window method over land surfaces. *Int. J. Remote Sens.* **1990**, *11*, 369–393. [CrossRef]
56. Wan, Z.M.; Dozier, J. A generalized split-window algorithm for retrieving land-surface temperature from space. *IEEE Trans. Geosci. Remote Sens.* **1996**, *34*, 892–905.
57. Coll, C.; Caselles, V. A split-window algorithm for land surface temperature from advanced very high resolution radiometer data: Validation and algorithm comparison. *J. Geophys. Res. Atmos.* **1997**, *102*, 16697–16713. [CrossRef]
58. Wan, Z.M.; Zhang, Y.L.; Zhang, Q.C.; Li, Z.L. Validation of the land-surface temperature products retrieved from Terra moderate resolution imaging spectroradiometer data. *Remote Sens. Environ.* **2002**, *83*, 163–180. [CrossRef]
59. Wan, Z.M. MODIS Land-Surface Temperature. Algorithm Theoretical Basis Document. 1999. Available online: http://modis.gsfc.nasa.gov/data/atbd/atbd_mod11.pdf (accessed on 19 September 2017).
60. Snyder, W.C.; Wan, Z.; Zhang, Y.; Feng, Y.Z. Classification-based emissivity for land surface temperature measurement from space. *Int. J. Remote Sens.* **1998**, *19*, 2753–2774. [CrossRef]

61. Wan, Z.M. *Collection-6 MODIS Land Surface Temperature Products. Users' Guide*; Eri, University of California: Santa Barbara, CA, USA, 2013.
62. Wan, Z.; Zhang, Y.; Zhang, Q.; Li, Z.L. Quality assessment and validation of the MODIS global land surface temperature. *Int. J. Remote Sens.* **2004**, *25*, 261–274. [CrossRef]
63. Wan, Z.M. New refinements and validation of the MODIS land-surface temperature/emissivity products. *Remote Sens. Environ.* **2008**, *112*, 59–74. [CrossRef]
64. Wan, Z. New refinements and validation of the collection-6 MODIS land-surface temperature/emissivity product. *Remote Sens. Environ.* **2014**, *140*, 36–45. [CrossRef]
65. Wan, Z.M. Mod11b3 MODIS/Terra Land Surface Temperature/Emissivity Monthly l3 Global 6km Sin Grid v006. NASA EOSDIS Land Processes DAAC. 2015. Available online: https://doi.Org/10.5067/modis/mod11b3.006 (accessed on 19 September 2017).
66. Prata, A. *Land Surface Temperature Measurement from Space: AATSR Algorithm Theoretical Basis Document*; Technical Report; CSIRO: Canberra, Australia, 2000; 27p.
67. Globtemperature Data Portal. Available online: http://data.globtemperature.info (accessed on 19 September 2017).
68. Ghent, D. *Land Surface Temperature Validation and Algorithm Verification*; Report to European Space Agency (UL-NILU-ESA-LST-VAV); European Space Agency: Paris, France, 2012.
69. Ghent, D.; Corlett, G.; Remedios, J. Advancing the AATSR land surface temperature retrieval with higher resolution auxiliary datasets: Part B—Validation. **2017**; in preparation.
70. Ninyerola, M.; Pons, X.; Roure, J.M. *Atlas Climático Digital de la Península Ibérica. Metodología y Aplicaciones en Bioclimatología y Geobotánica*; Universitat Autònoma de Barcelona: Bellaterra, Spain, 2005; 44p. Available online: http://opengis.uab.es/wms/iberia/pdf/acdpi.pdf (accessed on 19 September 2017).
71. Land Cover Map of Catalonia. CREAF–Generalitat de Catalunya. Available online: http://www.creaf.uab.cat/mcsc/usa/index.htm (accessed on 19 September 2017).
72. Atlas Climático Digital de Catalunya. UAB. Available online: http://www.opengis.uab.cat/acdc/espanol/es_presentacio.htm (accessed on 19 September 2017).